Tutor/s

Dr. Jose Antonio Padilla
Ciència de Materials i Química Física

Dr. Elena Xuriguera
Ciència de Materials i Química Física

Grau de Química

Treball Final de Grau

Characterization of FFF printed parts made of 3Y-TZP and Al_2O_3 filaments.
Caracterització de peces impreses per FFF de fils de 3Y-TZP i Al_2O_3.

Eloi Pozuelo Riera

June 2025

Universitat de Barcelona

B:KC Barcelona Knowledge Campus
Campus d'Excel·lència Internacional

REPORT

IDENTIFICATION AND REFLECTION ON THE SUSTAINABLE DEVELOPMENT GOALS (SDG)

In 2015, the United Nations (UN) adopted the 2030 Agenda for Sustainable Development, a global action plan consisting of 17 Sustainable Development Goals (SDGs) showed in Figure 1, and 169 specific targets. These goals provide a comprehensive framework to address the major social, economic and environmental challenges facing the planet, such as poverty, climate change, inequality, environmental degradation or universal access to health, education and technology. The SDGs are designed to be achieved in an integrated and universal way by 2030 and require the active collaboration of governments, businesses, academia and civil society. Each is interconnected with the others, promoting development that does not compromise resources and the well-being of future generations. The SDGs are structured around five key pillars: **People**, **Planet**, **Prosperity**, **Peace**, and **Partnership**, each representing a core area of focus for sustainable development.

***Figure 1**. The 17 Sustainable Development Goals (SDGs) established by the United Nations as part of the 2030 Agenda for Sustainable Development. Available at: https://www.un.org/sustainabledevelopment/sustainable-development-goals/*

The **People** pillar and the **Prosperity** pillar are the two areas under which this work can be classified, based on the Sustainable Development Goals (SDGs) to which it is related. These are:

SDG 3 - Ensure healthy lives and promote well-being for all at all ages

SDG 3 (Figure 2, a) aims to improve global health, increase access to health technologies and strengthen health systems through innovation and sustainable development. This project contributes directly to this goal by focusing on the investigation and optimisation of ceramic materials, such as partially yttria-stabilised zirconia (YSZ) and alumina (Al_2O_3), for use in customised biomedical implants, such as hip prostheses. Furthermore, nowadays, hip prostheses can be manufactured using 3D printing technology. This allows the production of customized parts adapted to each patient's anatomy, which can lead to greater biocompatibility, a lower risk of post-operative complications, and more efficient healing.

SDG 9 - Build resilient infrastructure, promote inclusive and sustainable industrialisation and foster innovation

SDG 9 promotes the adoption of advanced and innovative technologies that drive sustainable industrialisation. Additive manufacturing (AM) commonly known as 3D printing, is a key component of the research and a fundamental tool of the Fourth Industrial Revolution. 3D printing of technical ceramics, using filaments such as those developed by Zetamix, represents a disruptive innovation in the biomedical and materials sectors, enabling the creation of complex structures with high precision and reproducibility. For this reason, SDG 9 can be clearly related to the context of the research.

SDG 12 - Ensure sustainable consumption and production

SDG 12 aims to reduce the environmental impact of production processes and promote a circular economy. In this context, the work falls within the framework of responsible production as it uses AM, an approach that contrasts with traditional subtractive manufacturing (SM). While the latter involves machining blocks of material, generating a large amount of waste, 3D printing deposits material layer by layer, optimising resource consumption and minimising waste.

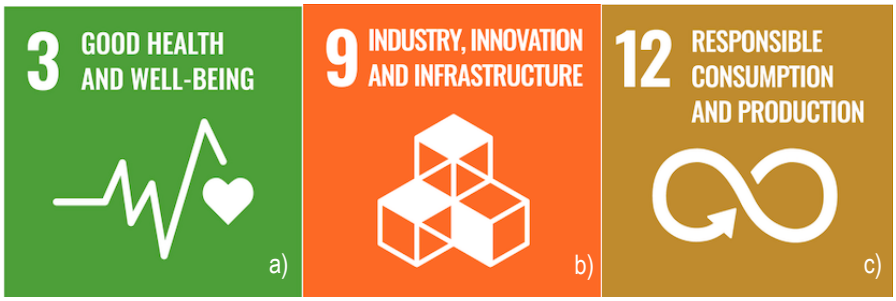

Figure 2. *SDG icons: a)* ***SDG 3*** *- Ensure healthy lives and promote well-being for all at all ages; b)* ***SDG 9*** *- Build resilient infrastructure, promote inclusive and sustainable industrialization, and foster innovation; c)* ***SDG 12*** *- Ensure sustainable consumption and production. (Images adapted from the United Nations Sustainable Development Goals platform: https://www.un.org/sustainabledevelopment/sustainable-development-goals/).*

CONTENTS

1. SUMMARY

This study focuses on determining the optimal thermal treatment conditions for YSZ and Al_2O_3 samples manufactured using 3D printing technology through Fused Filament Fabrication (FFF), with the aim of achieving superior mechanical and microstructural properties while addressing known issues such as Low Temperature Degradation (LTD) in the case of YSZ.

Thermogravimetric analysis (TGA) guided the design of the thermal profiles to ensure controlled removal of organic binders without compromising the structural integrity of the samples. Mass loss and volumetric shrinkage were characterized, confirming that the debinding process removes most of the organic components, while sintering promotes densification. Densification and porosity results were in good agreement with the specifications provided by the supplier (Zetamix) for YSZ, especially after one hour of sintering at 1500 °C, whereas alumina samples showed partially divergent trends, likely due to limited processing conditions.

Flexural strength tests revealed that alumina samples closely matched the mechanical performance predicted by Zetamix, while YSZ samples showed lower values due to the presence of microcracks, as confirmed by SEM analysis. Rheological characterization showed a desirable shear-thinning behavior and appropriate yield stress values for both ceramic filaments, confirming their suitability for extrusion-based additive manufacturing. Microstructural studies using FE-SEM and EDS detected alumina inclusions in the YSZ samples, possibly related to mechanical defects, while alumina samples showed homogeneous microstructures with larger grain sizes correlating to higher strength.

Overall, this study highlights the critical role of thermal process control in balancing densification, microstructure, and mechanical properties. The results support the potential of these ceramic materials for demanding functional applications, with special emphasis on biomedical implants such as hip prostheses. Further research is recommended involving advanced microstructural analysis, broader mechanical testing, and optimization of 3D printing parameters to mitigate defects and improve final part performance.

Keywords: 3D printing, Fused Filament Fabrication (FFF), Zetamix, YSZ, 3Y-TZP, Al_2O_3, Low Degradation Temperature (LTD), debinding, sintering.

2. RESUM

Aquest treball es centra en la determinació de les condicions òptimes de tractament tèrmic per a mostres de YSZ i Al_2O_3 fabricades mitjançant impressió 3D amb tecnologia Fused Filament Fabrication (FFF), amb l'objectiu d'obtenir propietats mecàniques i microestructurals superiors, i reduir problemàtiques conegudes com la degradació a baixa temperatura (LTD) en el cas de la YSZ.

L'anàlisi termogravimètric (TGA) va guiar el disseny dels perfils tèrmics per assegurar l'eliminació controlada dels aglutinants orgànics sense comprometre la integritat de les mostres. Es va caracteritzar la pèrdua de massa i la contracció volumètrica, confirmant que el desaglomerat elimina la major part dels components orgànics mentre que la sinterització promou la densificació. Els resultats de densificació i porositat van mostrar una bona coincidència amb les especificacions del proveïdor (Zetamix) per a YSZ, especialment després d'una hora de sinterització a 1500 °C, mentre que les mostres d'alúmina van mostrar tendències parcialment divergents, probablement a causa de les condicions limitades de processament provades.

Els assajos de resistència a flexió van revelar que les mostres d'alúmina s'acostaven al rendiment mecànic predit per Zetamix, mentre que les mostres de YSZ van obtenir resultats inferiors a causa de la presència de micro-esquerdes identificades mitjançant l'anàlisi SEM. La caracterització reològica va mostrar un comportament de pèrdua de viscositat amb el cisallament desitjable i valors adequats de límit de fluïdesa per a ambdós filaments ceràmics, confirmant la seva idoneïtat per a la fabricació additiva per extrusió. Els estudis microestructurals mitjançant la microscopia electrònica d'escaneig amb emissió de camp (FE-SEM) van detectar inclusions d'alúmina en les mostres de YSZ, possiblement relacionades amb defectes mecànics, mentre que les mostres d'alúmina van mostrar microestructures homogènies amb grandàries de gra majors que correlacionen amb una major resistència.

En conjunt, aquest estudi destaca el paper fonamental del control dels processos tèrmics per equilibrar la densificació, la microestructura i les propietats mecàniques. Els resultats recolzen el potencial d'aquests materials ceràmics per a aplicacions funcionals exigents, amb especial èmfasi en implants biomèdics com les pròtesis de maluc. Es recomana ampliar la investigació amb anàlisis microestructurals avançades, assajos mecànics més extensos i optimització dels paràmetres d'impressió 3D per mitigar defectes i millorar el rendiment final de les peces.

Paraules clau: Impresió 3D, Fused Filament Fabrication (FFF), Zetamix, YSZ, 3Y-TZP, Al_2O_3, degradació a baixa temperatura (LTD), desaglomerat, sinterització.

3. INTRODUCTION

Over the years, various studies have shown a continuous increase in life expectancy. Consequently, it becomes increasingly important to ensure that these additional years are accompanied by a good quality of life, which requires greater attention to the care and preservation of the human body. Thanks to medicine, which has been considered a science since the 19th century, people can now live longer lives with a guaranteed quality of life due to new techniques and scientific discoveries. Medicine has undergone many advances, but since the 20th century, one field has emerged as particularly important: biomedicine [1].

Biomedicine is a discipline that combines biology, medicine, and chemistry to study human diseases, their causes, mechanisms, and possible treatments [2]. It is based on scientific principles and the use of advanced technologies such as genetics, molecular biology, bioengineering, and biomedical chemistry. The latter is essential for the development of new drugs, therapies, and diagnostic tools aimed at improving human health. One of the most significant areas within biomedicine is the development of prostheses, medical devices designed to replace body structures that have lost their functionality due to disease, trauma, or natural wear. There are different types of prostheses used to replace various parts of the body when they have lost their function due to disease, injury, or wear. Among the most common are joint prostheses, such as hip and knee replacements, which substitute damaged joints to restore mobility; dental prostheses, which replace missing teeth; limb prostheses, which replace amputated limbs to restore functionality; and internal prostheses, such as pacemakers or stents, which support specific functions within the body. This field is in continuous development, as the need for prosthetic implantation increases over time and can be observed in Figure 3, which shows the number of hip arthroplasties performed in Catalonia from 2005 to 2014.

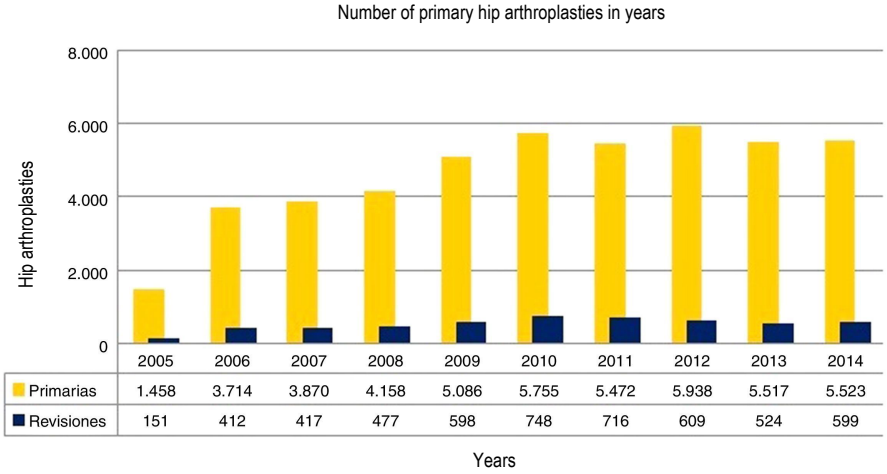

	2005	2006	2007	2008	2009	2010	2011	2012	2013	2014
Primarias	1.458	3.714	3.870	4.158	5.086	5.755	5.472	5.938	5.517	5.523
Revisiones	151	412	417	477	598	748	716	609	524	599

Figure 3. Number of primary hip arthroplasties performed in Catalonia between 2005 and 2014.
(Image adapted from Montero-Muñoz et al., *Revista Española de Cirugía Ortopédica y Traumatología*, 2019)

As shown in Figure 3, hip prosthesis implantation procedures have become progressively more common in recent years. These prosthetic devices are designed to restore the function of the joint when the biological structures can no longer perform adequately, allowing patients to regain mobility and continue walking independently. A typical hip prosthesis consists of three key components: the femoral stem, femoral head, the plastic liner and acetabular component (Figure 4). The femoral stem is inserted into the femur and can be fixed to the bone using orthopaedic cement or through a method called osseointegration, where an uncemented stem integrates biologically with the bone. The femoral head is a spherical component that replaces the head of the femur, articulating with the acetabular cup which is placed in the acetabulum of the pelvis to house the femoral head [3].

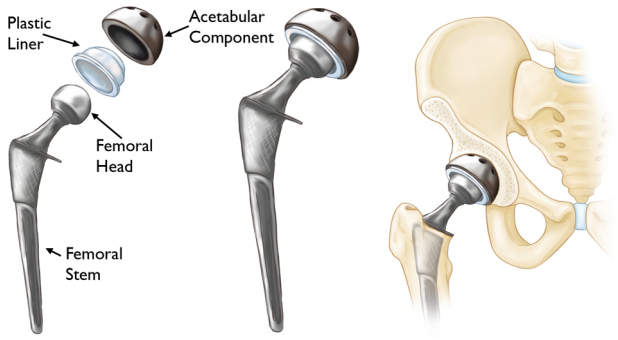

Figure 4. Components of a total hip prosthesis and their biomechanical integration within the human body.
(Image adapted from American Academy of Orthopaedic Surgeons, *OrthoInfo*, https://orthoinfo.aaos.org/en/treatment/revision-total-hip-replacement/)

3.1 MATERIALS FOR PROSTHESES

The materials used in hip prostheses have evolved significantly to enhance durability, biocompatibility, and functionality. Common materials include metals, such as titanium and cobalt-chromium alloys, which offer excellent mechanical strength and biocompatibility [3]. These metals are typically used in components that are in direct contact with bone. Ceramics, particularly zirconium oxide (ZrO_2) and aluminium oxide (Al_2O_3), have gained popularity due to their remarkable wear resistance and reduced friction [3,4]. Commonly are used for the femoral head and acetabular cup, as it minimizes wear on the articulating surfaces and enhances the prosthesis's longevity. Additionally, high-density polymers, such as polyethylene, are widely used for the acetabular cup due to their cushioning properties and wear resistance.

In addition to these material and manufacturing advancements, the application of nanotechnology and surface treatments such as antibacterial coatings have further improved the integration of prostheses with bone. These innovations not only help reduce the risk of infection but also promote faster recovery and a more stable implant over time, enhancing the overall success rate of hip replacement surgeries [5].

Zirconium oxide also known as zirconia is obtained directly from the natural mineral, maintains this monoclinic structure at room temperature, in which each zirconium atom is coordinated with seven oxygen atoms in its surroundings [6].

Is widely used for its high toughness, good mechanical properties and crack resistance [4]. Zirconia exhibits polymorphism, with three allotropic forms: monoclinic (a), tetragonal (b) and cubic (c) [7] (Figure 5). Each of these forms is stabilised at different temperatures and can transform from one to the other depending on environmental conditions. Zirconia has a monoclinic crystalline structure at room temperature. When heated, this structure transforms into a tetragonal structure at 1170 °C and then into a cubic fluorite-like structure at about 2370 °C.

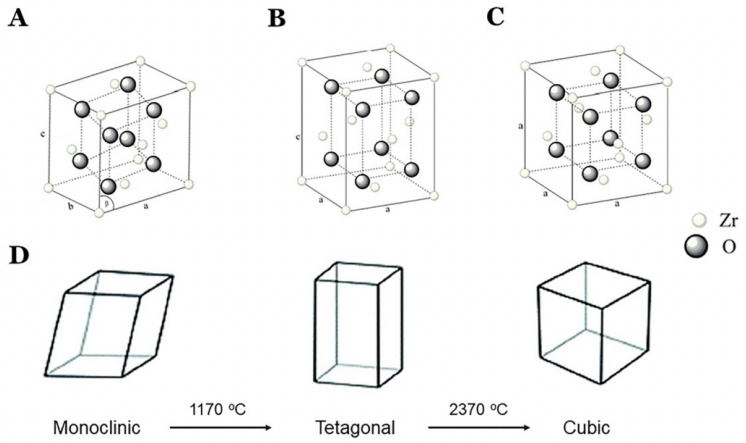

***Figure 5**. Polymorphisms of zirconia: (A) monoclinic, (B) tetragonal, (C) cubic, and (D) transformation phases.*
(Image adapted from Kongkiatkamon et al., PeerJ 11: e15669 2023.)

When temperature decrease, there is a change in the structure and the transformation from the tetragonal to the monoclinic phase leads to a volumetric expansion of 5% [7], which can induce internal stresses resulting in cracks or fractures in the material. To avoid these drawbacks and stabilize the tetragonal form, stabilising oxides, such as yttrium oxide (Y_2O_3), are added to the crystal lattice of zirconia [8]. This stabilisation allows the tetragonal and cubic phases to remain stable at room temperature, improving the mechanical properties of the material, such as its toughness and resistance to crack propagation. The addition of Y_2O_3 generates oxygen vacancies in the crystal lattice (Figure 6), contributing to the stabilisation of the high-temperature phases at lower temperatures [9]. This phenomenon is critical for applications requiring high mechanical strength and thermal stability, such as biomedical prosthetics and thermal coatings.

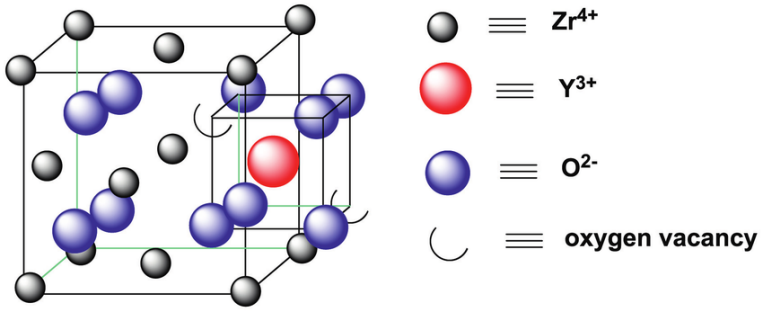

***Figure 6**. Image of the crystal structure of yttria-stabilized zirconia (YSZ), showing the substitution of Zr^{4+} ions by Y^{3+} and the resulting oxygen vacancies required for charge neutrality. (Image adapted from Murali Rao, H. et al., IntechOpen, 2023. doi:10.5772/intechopen.11160)*

In addition, studies have shown that the grain size of zirconia influences its phase stability. Smaller grains can stabilise the tetragonal phase at lower temperatures without the need for additives, due to the increased surface energy associated with decreasing grain size.

In humid environments, such as inside the human body, yttria-stabilized tetragonal zirconia polycrystal (Y-TZP) tends to experiment the low temperature degradation (LTD) [9]. LTD is induced by polar molecules, typically water, dissociating and oxygen-containing species occupying the oxygen vacancies in the crystal lattice [9]. Therefore, the tetragonal phase destabilises and transforms into a monoclinic phase without any external mechanical stress. The volumetric expansion of the transformed domains puts the surface of the components under compressive stress, which causes the grain boundaries to open, facilitating the penetration of fluids into the material [9]. To mitigate this phenomenon, various strategies have been proposed. One of the most effective is the incorporation of co-stabilizing such as aluminium or cerium oxide, which enhance resistance to phase transformation triggered by moisture and temperature [10]. In addition, reducing the grain size has been shown to limit the propagation of the monoclinic phase, thereby increasing the material's stability [11]. On the other hand, advanced manufacturing techniques, such as controlled sintering or silica infiltration via atomic layer deposition (ALD), have shown promising results by creating surface barriers that hinder moisture penetration and slow down degradation [12].

Aluminium oxide (also known as alumina, Al_2O_3) is an important ceramic material in the manufacture of hip prostheses thanks to its excellent mechanical, chemical and biocompatible properties. Its corundum-type crystalline structure comprises a compact hexagonal lattice, with aluminium ions occupying two-thirds of the octahedral sites and oxygen ions forming a closed hexagonal structure (see Figure 7). This configuration gives alumina high density, hardness and thermal stability — essential attributes for withstanding the loads and wear present in the hip joint. The material's purity, typically exceeding 99.5%, is crucial for maintaining its mechanical properties and ensuring biocompatibility by minimising impurities that could impact its performance in the human body [13].

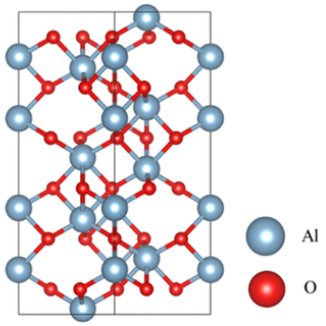

***Figure 7**. Image of the corundum-type crystal structure of alumina (α-Al_2O_3), showing the hexagonal close-packed arrangement of oxygen atoms (red spheres) and the occupation of octahedral sites by aluminum ions (gray spheres). (Image adapted from Ramogayana, B. et al., ACS Omega 2021, 6, 29577-29587)*

Alumina can exist in several phases or polymorphs, depending on the arrangement of atoms in its crystal structure. Among these phases, alpha (α), gamma (γ), delta (δ) and theta (θ) stand out, among others. Alpha alumina (α-Al_2O_3) is the most stable form and is found naturally in corundum ore. It has a compact hexagonal corundum-type crystalline structure, characterised by its density, order and rigidity, which gives it high hardness, mechanical strength and thermal stability.

Due to these superior properties, it is the phase used in technical and biomedical applications, such as in the manufacture of hip prostheses [14]. On the other hand, the gamma, delta and theta phases are metastable and form under specific conditions, such as during synthesis or calcination at lower temperatures. These phases have more disordered and porous structures, with inferior mechanical and thermal properties, and are therefore not used in applications that require high performance, such as biomedical implants [15].

Among the most notable properties of alumina are its high hardness, compressive strength, rigidity, and excellent wear and corrosion resistance. However, these properties can be affected by the porosity of the material, which is a critical factor in the durability of implants. An increase in porosity significantly reduces mechanical strength and elasticity, compromising the material's ability to withstand cyclic and prolonged loads, such as those experienced by a hip prosthesis during movement. For this reason, manufacturing processes, including advanced techniques such as 3D printing, must be optimised to reduce porosity and obtain dense and homogeneous parts [16]. In addition to its mechanical strength, alumina has high biocompatibility, meaning that it does not induce inflammatory responses or toxicity in surrounding tissues. This characteristic is essential to ensure the integration of the implant with the bone and prevent rejection or post-operative complications. The combination of its hardness and low coefficient of friction reduces wear at the joint interface, decreasing the generation of particles that can cause inflammation, osteolysis and eventual implant failure, which in turn prolongs the life of the prosthesis and improves the patient's quality of life [13].

Recently, 3D printing has enabled the manufacture of alumina implants with complex and customised geometries, optimising anatomical adaptation and integration with the bone. This technological advance offers new possibilities for improving the functionality of prostheses and reducing complications arising from poor adaptation or premature wear [17]. However, the inherent fragility of alumina and the difficulty in controlling its porosity remain significant challenges. To overcome these limitations, composite ceramics incorporating stabilised zirconia particles have been developed, improving fracture toughness without sacrificing hardness or biocompatibility, thus offering more resistant and reliable materials for medical applications [17].

3.2 Prostheses Manufacturing

In recent decades, the manufacturing process for hip prostheses using the materials has been subtractive manufacturing (SM) 3D printing technology (see Figure 8 A). This process involves starting from a block of material and removing the necessary amounts to shape the final piece.

However, recently AM has begun to be used (see Figure 1 B), a technique in which the piece is created from raw material by adding it layer by layer until the final geometry is obtained [18]. These manufacturing processes have sparked a revolution in the biomedical field due to the possibility of producing customized structures from biocompatible materials, allowing adaptation to the

specific anatomical characteristics of each patient and significantly improving both implant integration and performance. Customized manufacturing optimizes the function of the prosthesis and reduces the risk of post-operative complications by improving alignment and fit [19].

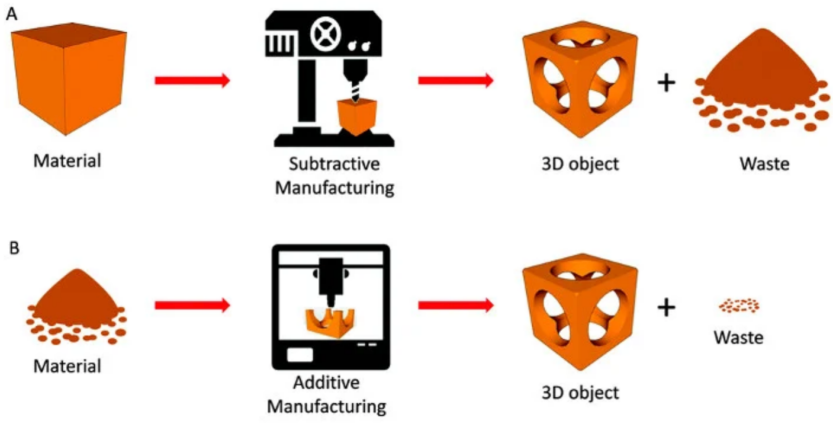

Figure 8. *Differences between subtractive and additive manufacturing.*
(Extracted from Bitfab. (2020). Qué es la fabricación aditiva y cómo funciona. https://bitfab.io/es/blog/fabricacion-aditiva/)

One of the main advantages of this technology is its time and resource efficiency, as no specific moulds or tooling are needed for each new product, which considerably reduces development time and initial costs [20]. This makes it a key tool for rapid prototyping and part customisation. In addition, the environmental impact of AM can be lower compared to traditional processes, as material waste is minimised, and it often enables the production of lighter components, thus improving energy efficiency in industrial applications [21]. The combination of sustainability, flexibility and efficiency makes AM one of the pillars of the fourth industrial revolution or Industry 4.0 [22].

Figure 9 provides a graphical summary of the AM process in general terms. Starts with the creation of a three-dimensional digital model of the desired object using computer-aided design (CAD) software as SolidWorks. The next step is to convert the CAD file into a program such as Standard Tessellation Language (STL) [18], with the aim of creating a printing program that the printer will follow. Once the model is created, it is processed by slicing software (UltiMarker Cura, etc...), which transforms the model into horizontal layers and configures the printing parameters such as speed, temperature or layer thickness. This step is crucial to ensure the quality and success of the final print [23]. During printing, the material is deposited layer by layer according to the digital model. This process is repeated until the object is fully formed. At the end, post-processing processes, such as support removal and heat treatment, are usually performed to improve the finish and final properties of the part [24].

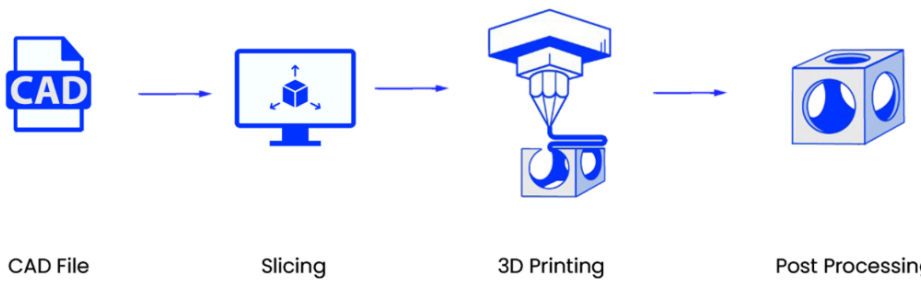

Figure 9. *Additive manufacturing process. (Extracted from:Roboze. (2023). Introducción a la fabricación aditiva: definición, funcionamiento y aplicaciones. https://www.roboze.com/en/resources/introduction-to-additive-manufacturing-definition-how-it-works-applications)*

In the biomedical field, AM has opened new possibilities for the manufacture of customised components such as hip implants and other medical devices tailored to the specific needs of each patient [25]. One of the most outstanding advantages of this technology is the precise control over the geometry, size and distribution of the material in the printed parts, resulting in structures with high

functionality and biocompatibility [22]. This level of customisation and precision is particularly relevant in medical applications, where the shape and properties of the part can directly influence the efficacy of the treatment and the patient's quality of life [26]. Thus, AM not only represents a revolution in the way we produce objects, also in how we can improve people's lives through technology [20].

As shown in Figure 10, there are seven families within 3D printing. Within the extrusion family, one of the most affordable and accessible manufacturing methods is Fused Filament Fabrication (FFF), which is used to synthesize YSZ and Al_2O_3 components for hip prostheses.

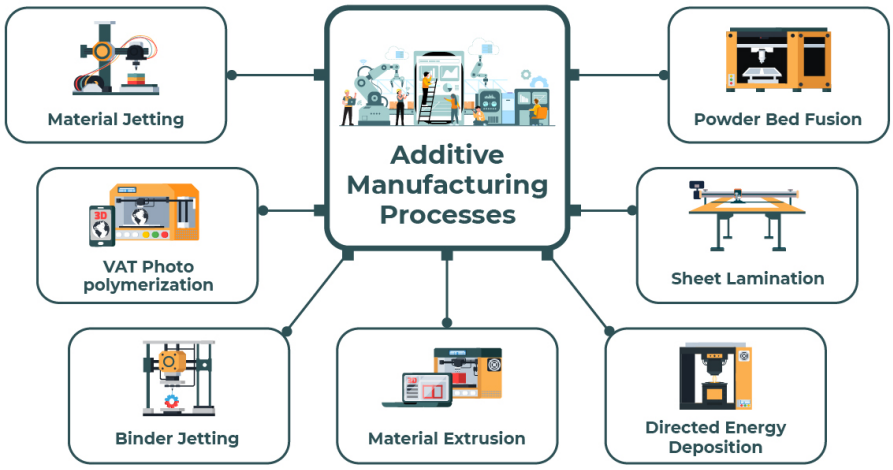

Figure 10. *Main families of Additive Manufacturing (AM) technologies, classified into seven core processes.*
(Adapted from: Symmetry Electronics. (2022). Defining Additive Manufacturing.https://www.symmetryelectronics.com/blog/defining-additive-manufacturing/)

FFF is a 3D printing technology based on the extrusion of a thermoplastic material, usually in the form of a filament, which is heated, melted, and deposited layer by layer through a nozzle to form a part (see Figure 11). Although it was originally developed for prototyping purposes, it is now also used to produce final components. During the process, the molten material is pushed by a feeding system and flows at a constant rate, maintaining uniform pressure, speed, and cross-sectional diameter, which ensures high precision in the geometry of the printed part. This technique is notable for its simplicity, low cost, and ability to efficiently produce complex structures [27]

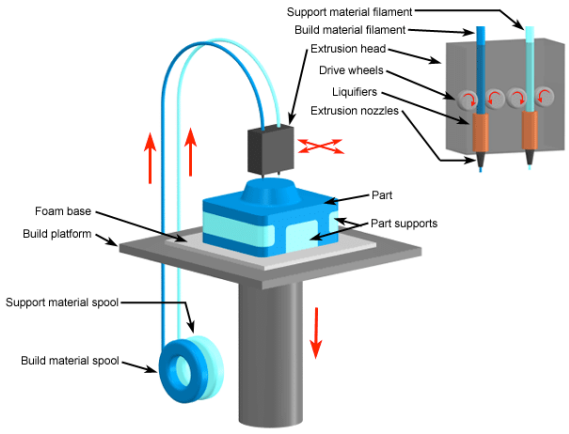

Figure 11. *Schematic representation of the working principle of Fused Filament Fabrication (FFF).*
(Image extracted from: Dhal, Kashish. (2018). On the Development and Integration of Pneumatic Extrusion Module and a Methodology to Identify Process Parameters for Additive Manufacturing using Machine Learning. 10.13140/RG.2.2.27244.31364.)

3.3 THERMAL TREATMENTS IN FFF FOR CERAMIC-LOADED MATERIALS

After manufacturing using 3D printing techniques, ceramic parts also known as green printed, require a consolidation process showed in figure 12, to achieve optimum mechanical and structural properties as specified. This process is carried out in two essential stages: debinding and sintering and obtain sintered body. Both stages are crucial to guarantee the final quality of the implant, especially in biomedical applications such as dental prostheses or hip implants, where mechanical integrity, density and biocompatibility are essential requirements.

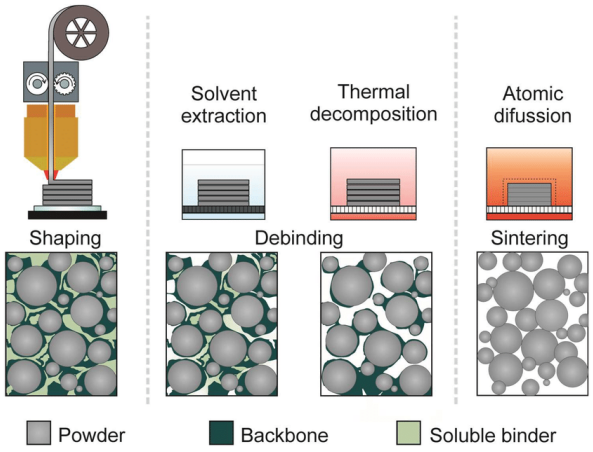

***Figure 12**. Post-printing treatment with solvent and thermal decomposition. (Image extracted from: Gonzalez-Gutierrez J, et al. (2018) Materials, 11(5): 840).*

3.3.1 Debinding

In the context of AM of ceramic materials, the debinding process is a critical step to ensure the structural integrity of the final component. During the filament fabrication, organic binders are essential to give cohesion to the ceramic particles. However, their permanence in the part can seriously compromise its subsequent consolidation, so they must be removed in a controlled and gradual manner to avoid the appearance of cracks, deformations or collapses in the green part [28].

Technical literature identifies three main debinding methods: thermal, solvent and catalytic. Thermal debinding removes the binder by heating the part until the organic material decomposes and evaporates. Solvent debinding dissolves the binder using a liquid solvent that penetrates and extracts it from the piece. Catalytic debinding employs a chemical catalyst to break down the binder at lower temperatures than thermal methods, enabling gentler removal. The choice of which depends on both the nature of the binder and the required properties of the final product.

For example, solvent debinding followed by a thermal step has been shown to reduce the incidence of defects and improve microstructural homogeneity in ceramics such as alumina [29]. In addition, recent studies emphasise the need for precise control of temperature, atmosphere and process kinetics, as abrupt or aggressive binder removal creates internal stresses that can lead to micro-fractures, pore opening or loss of geometry [30]. This phenomenon is particularly relevant in technologies such as stereolithography, where the fine geometry and complexity of printed structures require carefully designed thermal processes [31].

Finally, the success of the debinding process directly determines the efficiency of subsequent sintering and thus the densification, mechanical strength and functionality of the final ceramic component, key aspects for high-performance applications such as biomedical implants or wear-intensive parts [32].

3.3.2 Sintering

Once the binder has been removed, the next fundamental step in the AM of ceramic components is thermal sintering, the final consolidation process. In this stage, the ceramic particles are exposed to high temperatures, allowing them to coalesce by diffusion in the solid state. This coalescence results in a dense material with a refined microstructure and mechanical properties suitable for functional applications, particularly in the biomedical field [28].

The success of the sintering process is highly dependent on the precision with which the thermal parameters are controlled. Variables such as maximum temperature, type of atmosphere (inert or reducing), heating rate and thermal hold time must be carefully regulated. Any deviation can cause structural defects such as deformation, excessive shrinkage or internal porosity, which would compromise the integrity and functionality of the implant [32]. There are three main types of sintering techniques commonly used: conventional resistance furnace sintering, microwave sintering [33], and Spark Plasma Sintering (SPS) [34]. Among these, conventional resistance furnace sintering is the most widely employed due to its industrial scalability and ease of operation. However, this method requires long processing times and can cause internal thermal gradients that negatively impact the uniformity of the material [28]. The choice of sintering method affects not only density and mechanical strength, but also aspects such as biocompatibility, wear resistance and chemical stability of the final component. It is therefore essential to integrate materials science, thermodynamics and biomedical design criteria in the selection of the most appropriate sintering conditions.

As previously mentioned, post-printing heat treatments are intended to remove the binders present in the samples and improve their mechanical and structural properties. During the decomposition of these binders, the organic matter transforms into carbon dioxide (CO_2) and water (H_2O), which then evaporate. This process creates voids in the material's structure that, if not properly controlled, can compromise its functional and mechanical properties. For this reason, it is essential to carry out a series of determinations and tests to verify that the required properties have been achieved. Excessive mass loss during the debinding process can increase the material's porosity, making densification more difficult and, consequently, reducing its mechanical strength and functional performance [35]. However, excessive densification can also be unfavorable, as it may hinder the integration of the implant with biological tissue. Therefore, it is essential to achieve an appropriate balance between density and porosity to ensure both mechanical performance and biointegration of the material [36]. In this regard, porous alumina ceramics represent a clear example: a homogeneous porous structure not only facilitates interaction with surrounding tissues but also maintains sufficiently stable mechanical properties for use in biomedical applications [37].

To evaluate these aspects, techniques such as thermogravimetric analysis (TGA) are used to define suitable thermal profiles during the debinding stage; rheology, which helps characterize the viscous behavior of the material during extrusion; and scanning electron microscopy (SEM), which is key for analyzing the microstructure, detecting defects, and validating dimensional fidelity. Additionally, the three-point bending test serves as a fundamental tool for quantifying the structural strength of ceramic pieces, allowing for the establishment of correlations between sintering conditions and final mechanical performance.

4. OBJECTIVES

MAIN OBJETIVE:

To determine the optimal thermal treatment conditions applied to samples printed using FFF technology, composed of YSZ and Al_2O_3, in order to achieve optimal mechanical and microstructural properties.

SECONDARY OBJETIVES

- To apply post-printing thermal treatments, including debinding and sintering, in order to eliminate the organic binders present in the FFF 3D-printed parts and to confer the necessary densification and structural stability.

- To characterize the sintered samples using various experimental techniques, evaluating key parameters such as dimensional shrinkage, mass loss, densification, and porosity. In addition, scanning electron microscopy (SEM), thermogravimetric analysis (TGA), rheological studies, and mechanical property testing will be carried out.

- To analyze and interpret the results obtained with the aim of establishing correlations between processing conditions and the final behavior of the materials.

5. EXPERIMENTAL SECTION

5.1. INITIAL SAMPLES

The zirconia samples used in this study were provided by the research group led by Dra. Irene Buj at the Escola Tècnica Superior d'Enginyeria Industrial de Barcelona (ETSEIB), Universitat Politècnica de Catalunya (UPC). These samples were designed and manufactured by 3D printing using model printers *Artilleri Gemini* and *Cumpro*, both specialised in the additive manufacturing of ceramic-based materials.

The materials used for the printing process were filaments from the Zetamix brand, as shown in Figure 13. The Zetamix Zirconia filament stabilised with 3 mol% yttria (3Y-TZP) (Figure 14.a) and the alumina filament (Al_2O_3) (Figure 14.b) b)

Figure 13. *Zetamix (a)zirconia and (b)alumina filaments. (Zetamix website, retrieved 26/05/2025, via zetamix.fr)*

Table 1*. Properties of Zetamix yarns based on Al_2O_3 and YSZ.*

Tipe of yarms	Final sintered density (%)	Density (g/cm³)	Bending strength (MPa)	Shrinkage during sintering (%)	Printing temperature (ºC)	Sintering temperature (ºC)
Al2O3	98–99	2,5	200–500	X/Y: 20,8±1%; Z: 23,2 ±1%	120	1550
3Y-TZP	98–99	3,5	400–1000	X/Y/Z: 21,5±1%	180	1475

In total, 37 pieces were fabricated using Zetamix filaments (see Table 2): 19 of yttria-stabilised zirconia and 18 of alumina. The printing process was carried out using a linear deposition scheme, with a nozzle diameter of 0.4 mm and a layer height of 0.2 mm. The filament used had a diameter of 1.75 mm. The printing speed was set to 8 mm/s, with a fill density (infill) of 85%, and a fusion temperature of 180 °C. These parameters were selected to ensure optimal extrusion stability and structural integrity of the printed ceramic samples (see Figure 15) prior to subsequent post-processing. After printing and prior to thermal treatments, the samples were immersed in acetone for a specific period at a controlled temperature at the UPC department to carry out a solvent debinding process. The samples obtained by the Fused Filament Fabrication have been exposed in this Table 2.

Table 2. *Samples obtained with FFF a) YSZ b) Al_2O_3*

	Bottom face	Lateral face	Top face
a)	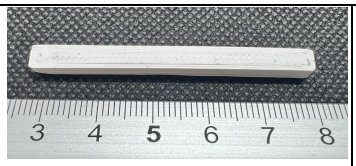	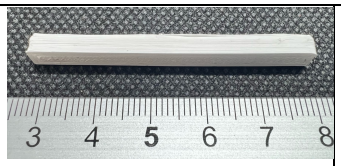	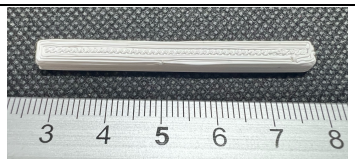
b)	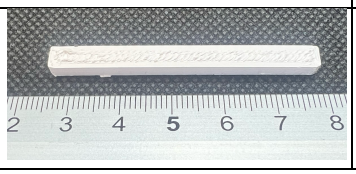	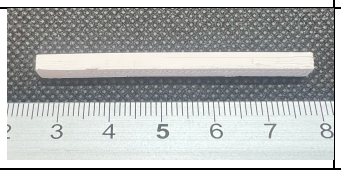	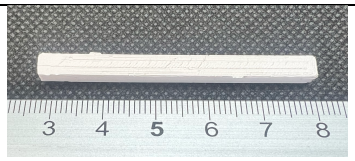

5.2. Debinding and Sintering of the samples

To optimise the removal of organic components and residual water present in the 'green' parts, and to enhance their mechanical properties, a specific post-printing treatment has been applied, varying according to the material used (YSZ or Al_2O_3). The post-printing process recommended by the supplier, Zetamix, begins with a solvent debinding stage, aimed at removing part of the organic binder content. This involves immersing the printed parts in an acetone bath for 6 hours at 40 °C, although the exact duration may depend on the geometry of the part. According to the supplier, this process typically results in a mass loss greater than 5%, indicating effective partial binder removal. After the immersion, the samples are dried for 2 hours at ambient conditions to allow complete evaporation of any residual solvent.

Following this, the samples undergo a thermal debinding and sintering process. The thermal cycle involves heating the samples up to 500 °C at a rate of 8 °C/h (debinding phase), after which the temperature is further increased for sintering. For YSZ, the target temperature is 1475 °C, and for alumina, 1550 °C, with both materials being held at their respective peak temperatures for 2 hours to ensure proper densification. The full thermal profile is illustrated in Figure 14.

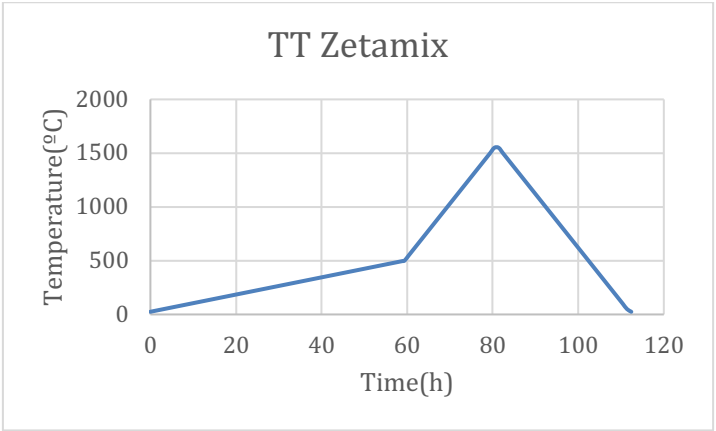

Figure 14. Thermal treatment profile recommended by Zetamix.

During the debinding and sintering processes, the organic compounds contained in the printed parts are expected to decompose and be released as gases, primarily CO_2 and H_2O. Ideally, these stages should be carried out in a furnace integrated into a fume hood to ensure safe evacuation of the emitted gases. However, due to the unavailability of a high-temperature furnace within such a ventilated system, the thermal treatment was divided into two distinct stages: Thermal Treatment 1 (TT1) for thermal debinding and Thermal Treatment 2 (TT2) for sintering. This separation allows for greater control over each stage and reduces the risk of contamination or defects caused by gas accumulation during heating. Furthermore, TT2 was conducted under varying sintering temperatures and holding times to obtain samples with different final microstructures (see Figure X). This approach enables a systematic comparison between processing conditions and their effects on the mechanical and microstructural properties of the YSZ and Al_2O_3 components. JB20 Hobersal 1100 °C

Table 3. *Thermal conditions applied in the different sintering treatments.*

YSZ			Al_2O_3		
Temperature (ºC)	**Time (h)**		**Temperature (ºC)**	**Time (h)**	
1450	1	3	1525	1	3
1475	1	3	1550	1	3
1500	1	3	1575	1	3

5.3 Final Measured Parameters

5.3.1 Shrinkage and Weight Loss

As previously mentioned, the use of 3D printing via FFF technology and ceramic-loaded filaments results in parts that require post-processing to achieve optimal mechanical properties**.** During the thermal treatment stages, the degradation of the organic binder creates voids within the material, which in turn leads to dimensional shrinkage. Therefore, evaluating both the shrinkage and mass loss is essential to assess the effectiveness and extent of the thermal treatments applied. For this purpose, dimensional measurements were taken using a high-precision digital calliper gauge (±0.01 mm), and mass measurements were obtained using an analytical balance (±0.001 g), both before and after the thermal treatment processes.

The linear shrinkage and weight loss were calculated using Eq.1 and Eq.2:

$$Shrinkage(\%) = \frac{Final\ value\ (mm) - Inital\ value(mm)}{Final\ value(mm)} \cdot 100 \qquad \textbf{Eq. 1}$$

$$Weight\ loss(\%) = \frac{Final\ weight(g) - Inital\ weight(g)}{Final\ weight(g)} \cdot 100 \qquad \textbf{Eq. 2}$$

5.3.2 Porosity and Desnification

In addition to dimensional and mass measurements, the evaluation of density and porosity is essential to understand the impact of thermal treatments on the final quality of ceramic parts. The decomposition of the organic binder during post-processing generates internal voids that, in addition to causing shrinkage, can directly affect the degree of densification of the material. These parameters

are particularly relevant when aiming to balance mechanical strength with biological integration, as required in biomedical applications such as hip prostheses. Determining the apparent density and estimating the total porosity of the sintered samples allows for a more accurate analysis of how processing conditions influence the final properties of the material.

An analytical balance equipped with a Sartorius YDK03 density determination kit was used to measure the weight of the sample in air, immersed in liquid, and after drying. These values are required to calculate the density, density on bulk, porosity and densification parameters using the following equations. (Eq. 3, Eq. 4, Eq. 5 and Eq. 6).

$$\rho\left(\frac{g}{cm^3}\right) = \frac{W_a \cdot (\rho_{water} - 0{,}0012)}{W_a - W_{fl}} + 0.0012 \qquad \textbf{Eq. 3}$$

$$Porosity(\%) = \frac{W_{a'} - W_a}{W_{a'} - W_{fl}} \cdot 100 \qquad \textbf{Eq. 4}$$

$$\rho_{bulk}\left(\frac{g}{cm^3}\right) = \frac{W_a \cdot \rho_{water}}{W_{a'} - W_{fl}} \qquad \textbf{Eq. 5}$$

$$Densification(\%) = 100 - Porosity \qquad \textbf{Eq. 6}$$

$W_a(g)$: $Dry\ weighing$ $W_{a'}(g)$: $Wet\ weighing$

$W_{fl}(g)$: $Immersion\ weighing$ $\rho_{water}\left(\frac{g}{cm^3}\right)$: $Water\ density$

5. 4 Mechanical Properties

Given that the materials subjected to thermal treatment are intended for biomedical applications, where they must withstand the loads and stresses of the human body, it is essential to evaluate their mechanical properties. This assessment determines the suitability of the material for real-world use. Therefore, flexural testing is performed as a key method to measure mechanical strength. Such tests are crucial to ensure that the manufactured components meet the reliability and safety standards required in critical applications like biomedical implants. To this end, the three-point bending test was carried out to assess the ability of the samples to withstand mechanical stress. This test makes it possible to determine the flexural strength of the material, i.e., its behavior under loads applied as bending moments. The comparative analysis of samples subjected to different sintering treatments allows identification of the thermal conditions that provide greater mechanical resistance, thus optimizing the manufacturing process. For the test, a universal testing machine from the manufacturer Zwick Roell was used.

It consists of applying a progressive load to the center of a prismatic specimen supported at two equidistant points (see Figure15). Given that the specimen's approximate diameter is 43 mm, a test span length of 40 mm is used, producing maximum tension in the lower part of the specimen and compression in the upper part. The loading speed is set at 0.5 mm/min. This type of test allows the determination of flexural strength. During the test, the applied force and the resulting deflection are recorded until the specimen fails or a pre-defined limit is reached. This method is particularly useful for brittle materials such as ceramics like zirconia and alumina, as it provides relevant information on their structural behavior under mechanical loading. In addition, by comparing the results of different heat treatments, it is possible to identify which ones provide greater flexural strength, which is essential in functional applications where components are subjected to significant mechanical stress.

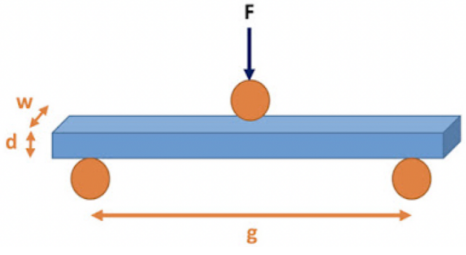

$d = Height$ $w = Thickness$ $g = Length$

Figure 15. Drawing of the three-point bending test.
(Taken from *Texture Analysis Professionals*, retrieved from textureanalysisprofessionals.blogspot.com)

5. 5 RHEOLOGY

As previously mentioned, the FFF technology was used to print the samples. This method relies on the extrusion of the selected filament, which is deposited layer by layer to form the final part. Since the material's behavior during extrusion directly affects the print quality, a rheological study was considered appropriate for both the 3Y-TZP and Al_2O_3 filaments to assess their processability.

The rheological analysis was performed using an HR20 rotational rheometer from TA Instruments, which provides data on viscosity as a function of shear stress—a key parameter for determining whether the material flows steadily and continuously through the printer nozzle. This information is essential to ensure uniform deposition, avoid defects such as clogging or geometric irregularities, and optimize printing parameters according to the specific characteristics of each filament.

5. 6 THERMOGRAVIMETRIC ANALYSIS

The removal of organic compounds and water content present in the printed samples requires a debinding process. This stage is essential, as it decomposes and eliminates the organic phases that serve as binders during printing, leaving behind a clean ceramic structure suitable for subsequent sintering.

The material supplier (Zetamix) provides a recommended temperature profile for this process; however, to validate this proposal and, if necessary, adapt it to the specific characteristics of the system used, a thermogravimetric analysis (TGA) was performed on both the 3Y-TZP and Al_2O_3 filaments. This technique enables a precise evaluation of mass loss as a function of temperature under a controlled atmosphere, allowing identification of the various thermal degradation stages of the organic compounds present in the filament. The test was conducted over a temperature range of 25 °C to 1000 °C using an SDT Q600 instrument from TA Instruments, specifically designed for simultaneous mass loss and heat flow analysis. The experiment was carried out in an oxidizing air atmosphere, enabling a detailed characterization of the thermal behavior of the binders and their response to oxidation. Based on these results, it is possible to confirm the suitability of the thermal profile suggested by the manufacturer or, if needed, define a more appropriate protocol to ensure efficient and controlled removal of binders, minimizing the risk of structural defects in the parts prior to sintering.

5. 7 SCANNING ELECTRON MICROSCOPY

To understand the properties acquired during the debinding and sintering processes and to correlate the different thermal treatment profiles with the final characteristics of the samples, scanning electron microscopy (SEM) analysis was performed. This technique is particularly valuable for characterising both the surface and internal microstructure of ceramic components, allowing for the assessment of critical factors such as pore distribution, microstructural homogeneity, and the presence of surface defects like cracks or residual cavities, which may compromise the material's performance.

A field emission scanning electron microscope (FE-SEM) was used for this analysis, offering significantly higher resolution compared to conventional SEM systems. This enhanced resolution enables high-definition imaging, even for ceramic materials with complex surfaces or low electrical conductivity. Additionally, a detailed grain size analysis was conducted to evaluate the degree of densification achieved and its potential influence on the mechanical and functional properties of the samples an especially important factor in structural and biomedical applications.

Prior to observation, all specimens were coated with a thin layer of graphite via cathodic sputtering to enhance their electrical conductivity and prevent surface charge accumulation, which could interfere with image acquisition. The coating was applied uniformly to preserve the original morphology and avoid altering microstructural features. Images were captured using Secondary Electron (SE) detection to analyze surface topography, Backscattered Electron (BSE) imaging to identify different phases based on atomic number contrast, and Energy Dispersive X-ray Spectroscopy (EDS) for qualitative compositional characterization. Observations were carried out at various magnifications and voltage of 20 kV.

6. CHARACTERIZATION

Thanks to the various experimental determinations, tests, and characterization techniques applied, it was possible to thoroughly evaluate the zirconia and alumina samples, with the aim of identifying their fundamental properties after thermal treatment. This evaluation has been structured into specific sections.

6. 1 THERMAL DEGRADATION STUDY

A thermogravimetric analysis (TGA) was performed for both the YSZ and alumina filaments, and the results are presented in Figures 16 and 18. As shown in the graphs, the mass losses indicate the temperatures at which the thermal degradations occur. As shown in the graph, the mass loss of the filaments made of YSZ occurs in three well-defined stages, with degradation peaks observed at approximately 330 °C, 453 °C, and 461 °C. The initial gradual decrease in mass can be attributed to the evaporation of residual water present in the sample. It is also worth noting that the final mass after thermal treatment stabilises at around 85 %, which aligns with the material composition specified by the supplier, indicating 86 % ceramic content (YSZ) and 14 % organic binder system.

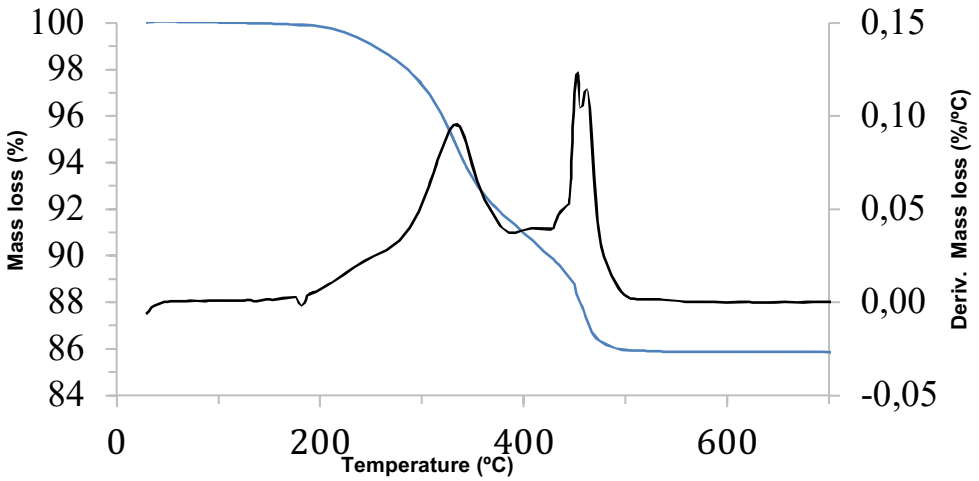

***Figure 16**. Results of YSZ TGA*

Based on the results obtained from the thermogravimetric analysis, the debinding stage was restructured using a more conservative approach to ensure a gradual and controlled decomposition of the binder system without compromising the structural integrity of the ceramic material. This adjustment aims to minimise the risk of structural defects during the thermal degradation of organic compounds. Consequently, a specific thermal treatment profile was defined (see Figure 17), in which each previously identified degradation peak is reached and held at its corresponding temperature for 6 hours.

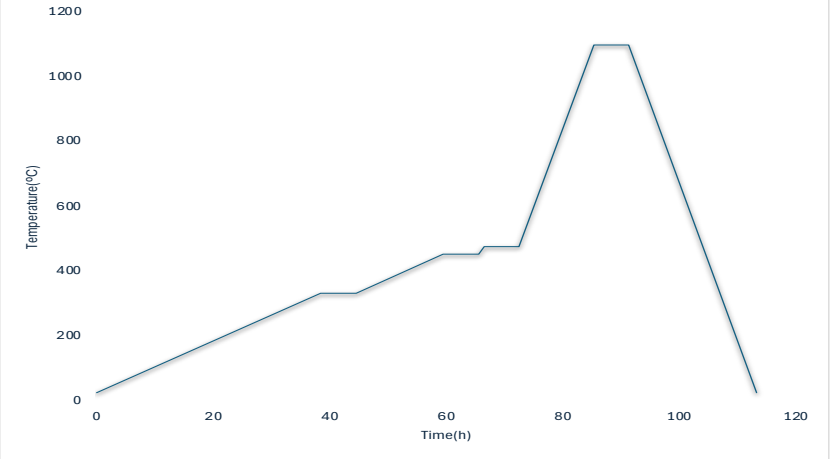

***Figure 17**. Graphic representation of the new debinding (TT.1YSZ)*

Similarly, the alumina filament was analyzed by identifying its degradation peaks and developing a more conservative debinding stage to ensure controlled degradation without compromising the structural integrity of the parts. In the TGA analysis of Al_2O_3 (Figure 18), degradation peaks were observed at 329 °C, 444 °C, and 525 °C. Additionally, a mass retention of 75% was recorded, slightly lower than the value provided by the manufacturer (83%) (Zetamix). However, it is worth noting that, as in the case of YSZ, the presence of ceramic material was confirmed at the end of the debinding phase.

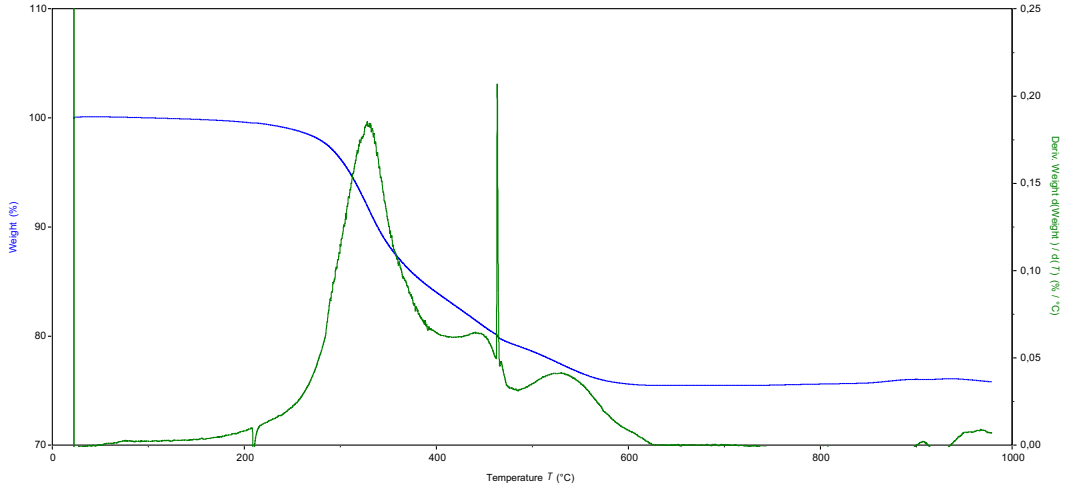

***Figure 18**. Results of Al_2O_3 TGA*

For the reasons previously discussed, a new heating ramp for the alumina has been developed (see Figure 19), specifically tailored to perform the debinding process in accordance with the type of binders contained in the material.

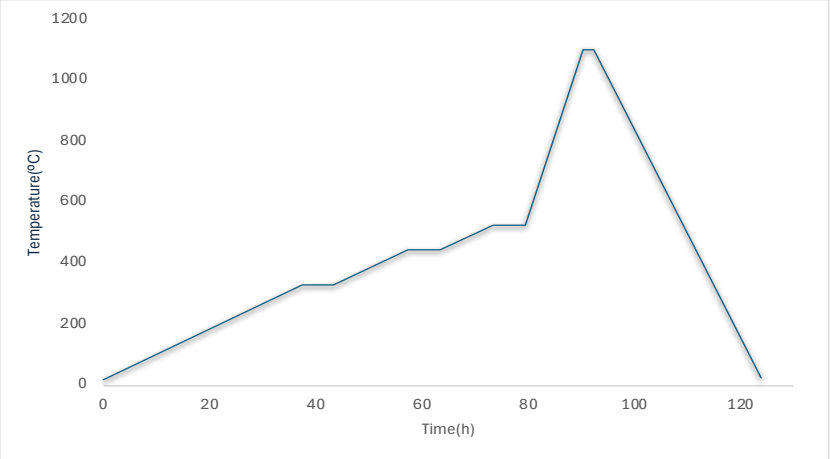

***Figure 19**. Grafic representation of the new debinding (TT.1 Al_2O_3)*

To complement the findings from the previous TGA analyses, a mass loss study was conducted for the two thermal processes applied to each sample, with the results presented in Table 4. This analysis provided valuable insights into the different thermal stages of the process. Specifically, it was observed that during the first thermal treatment, corresponding to debinding, most of the organic content in the samples was eliminated. In contrast, during the second treatment, corresponding to sintering, the mass loss was practically negligible, indicating that the organic fraction had already been removed beforehand, as expected. It is worth noting that, according to the data provided by Zetamix, the binder fraction is expected to be 14% for the YSZ filament and 17% for the alumina filament. Therefore, the mass losses observed during the debinding process are consistent with the supplier's specifications.

***Table 4**. Weight loss analysis*

Entrada	Material	Thermic condition	Initial Weight [g]	Weight TT1 [g]	Weight TT2 [g]	Weight Loss [%]
1	YSZ	1450ºC - 3h	2,9048	2,5382	2,5325	12,81

2	YSZ	1475ºC - 3h	3,0843	2,6759	2,6648	13,59
3	YSZ	1500ºC - 3h	2,8357	2,4965	2,4925	12,10
4	YSZ	1450ºC - 1h	3,1038	2,6937	2,6742	13,84
5	YSZ	1475ºC - 1h	3,1295	2,7012	2,6972	13,81
6	YSZ	1500ºC - 1h	3,1436	2,7334	2,71063	13,77
7	Al_2O_3	1575ºC - 3h	2,3287	1,9870	1,9715	14,33
8	Al_2O_3	1525ºC - 3h	2,0416	1,6730	1,6639	13,89

In parallel, a shrinkage analysis was conducted, with results detailed in Table 5. It was observed that volumetric shrinkage occurs primarily during the sintering stage, as expected. This behavior is attributed to diffusion phenomena and improved particle cohesion at high temperatures, which promote the consolidation of the ceramic structure. When comparing these results with the values reported by Zetamix (see Table 1), it becomes evident that the predicted shrinkage was not fully achieved. In contrast, during the debinding phase, no significant shrinkage was observed, as this stage involves the removal of organic components rather than material densification. Furthermore, although greater shrinkage was observed in the alumina samples, no definitive conclusions can be drawn regarding the influence of the applied thermal treatment on the extent of shrinkage.

***Table 5**. Contraction analysis of the samples*

Entrada	Material	Thermic condition	Height Contraction [%]	Width Contraction [%]	Length Contraction [%]
1	YSZ	1450ºC - 3h	18,8	18,2	19,5
2	YSZ	1475ºC - 3h	18,2	16,3	18,9
3	YSZ	1500ºC - 3h	19,5	19,1	18,8
4	YSZ	1450ºC - 1h	21,5	17,3	18,7
5	YSZ	1475ºC - 1h	20,7	18,7	19,4
6	YSZ	1500ºC - 1h	21,1	18,1	19,0
7	Al_2O_3	1575ºC - 3h	28,2	19,4	21,2
8	Al_2O_3	1525ºC - 3h	17,6	22,9	21,1

Finally, among the various characterizations performed, the analysis of densification and porosity stands out, as these parameters as mentioned in the introduction are critical for evaluating the mechanical properties and the suitability of the material for functional applications. These variations were analyzed as a function of temperature, holding time during the second thermal treatment, and the type of ceramic material used. It was observed that all three factors significantly influence densification and the evolution of porosity, directly affecting the mechanical and functional performance of the material. The combined effects of these variables are reflected in the results obtained, as illustrated in the graphs shown below (see Figures 20 and 22).

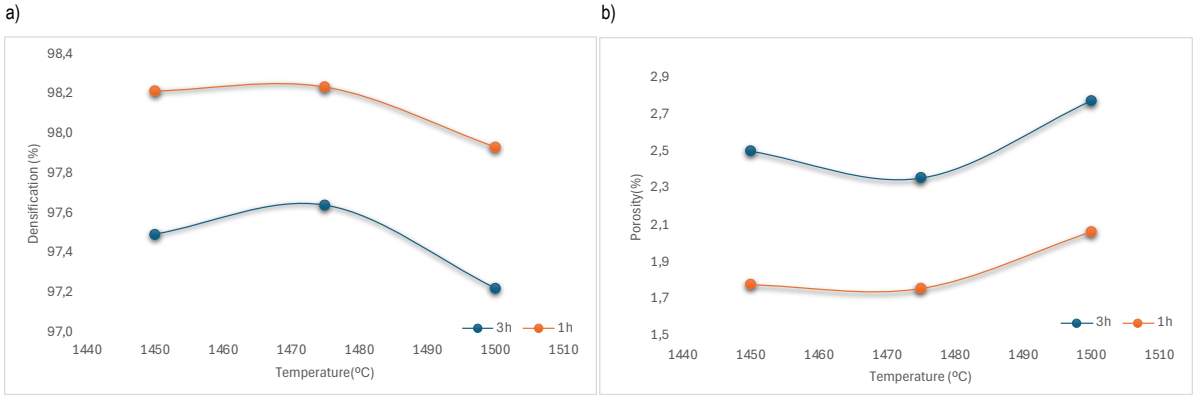

Figure 20. Variation in densification (a) and porosity (b) of YSZ samples versus sintering temperature.

Based on the results obtained, it can be concluded that, for YSZ, the best performance in terms of density and porosity is achieved when the samples are held at the sintering temperature for 1 hour. Under these conditions, the lowest porosity and highest density values were recorded, indicating better material compaction and a microstructure more suitable for functional applications. When analyzing the effect of temperature, it was observed that an increase of 25 °C improves densification and reduces porosity; however, a 50 °C increase leads to the opposite effect.

In the case of alumina, a different behavior was observed regarding the relationship between temperature, density, and porosity (see Figure 21). As the temperature increases, porosity increases while density decreases, suggesting a different structural evolution compared to YSZ. It is important to note that only two thermal conditions were evaluated in this case, and no variations in sintering time were applied, which limits the ability to establish a clear overall trend in the material's response to temperature.

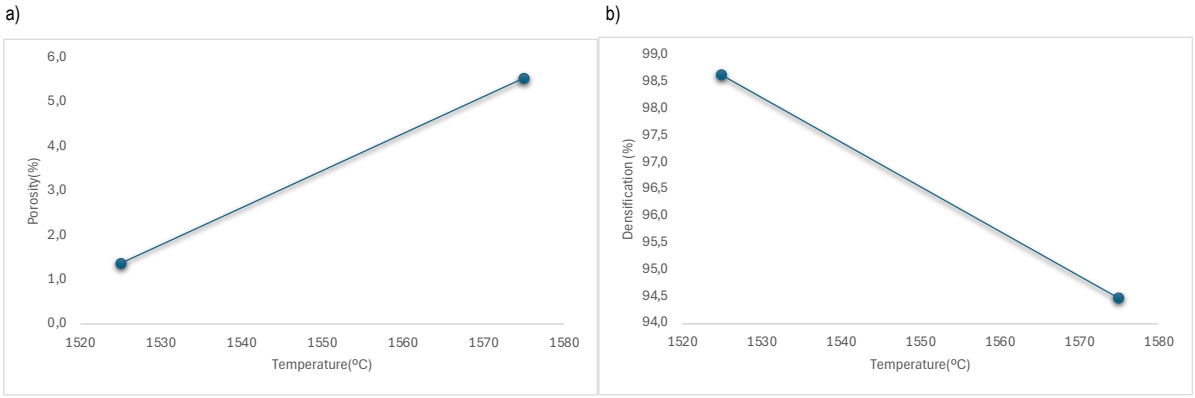

Figure 21. Variation in densification (a) and porosity (b) of Al_2O_3 samples versus sintering temperature.

Finally, it is worth highlighting the densities obtained according to the sintering time and temperature, as shown in Table 6. These values have been compared with those provided by Zetamix in their technical datasheet (see Table 1), leading to the conclusion that both the YSZ and Al_2O_3 samples correspond to the supplier's values, which state that the density of zirconia is higher than that of alumina. It is also noteworthy that, according to the table, varying the sintering temperature does not significantly change the density, whereas reducing the sintering time results in an improvement in density.

Table 6. Density values obtained according to the heat treatment.

Entrada	Material	Thermic condition	Density [g/cm]
1	YSZ	1450ºC - 3h	5,8
2	YSZ	1475ºC - 3h	5,8
3	YSZ	1500ºC - 3h	5,8
4	YSZ	1450ºC - 1h	5,9
5	YSZ	1475ºC - 1h	6,0
6	YSZ	1500ºC - 1h	6,0
7	Al_2O_3	1575ºC - 3h	4,9
8	Al_2O_3	1525ºC - 3h	3,9

6. 2 STUDY OF MECHANICAL PROPERTIES

As previously mentioned, analyzing the mechanical properties of the fabricated parts is essential to understand their structural behavior. Specifically, a higher flexural strength indicates a greater ability of the material to withstand loads without fracturing, which

is critical in functional applications subjected to repeated stresses, such as hip prostheses. For this reason, a flexural test was conducted to determine the flexural strength of each sample based on the applied thermal treatment and holding time. The obtained results are presented in Table 5 and illustrated in the corresponding graphs (see Figure 22).

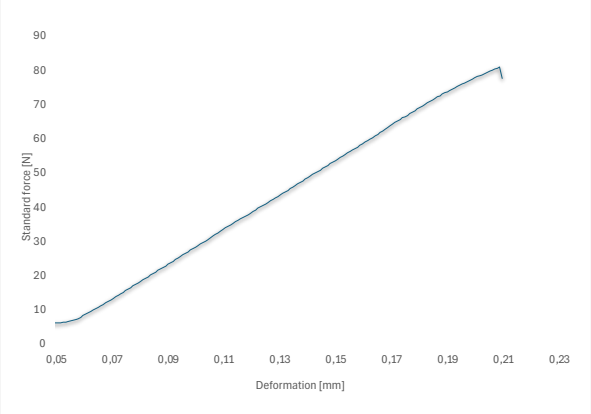

***Figure 22**. Graph obtained from the flexural test of sample 1450-3H-1*

Table 5. Fuerzas máximas y vending Strength de las diferentes muestras analizadas.

Entrada	Material	Thermic condition	Fmax [N]	Bending Strength [MPa]
1	YSZ	1450ºC - 3h	81,26	141,49
2	YSZ	1475ºC - 3h	56,64	97,63
3	YSZ	1500ºC - 3h	123,94	212,34
4	YSZ	1450ºC - 1h	18,14	30,22
5	YSZ	1475ºC - 1h	49,82	80,29
6	YSZ	1500ºC - 1h	72,94	122,80
7	Al_2O_3	1575ºC - 3h	290,09	560,15
8	Al_2O_3	1550ºC - 3h	84,51	153,30

When analysing the results, it has not been possible to establish relationships between the YSZ samples and their sintering temperatures and times, as they present very different values for bending strength and maximum strength. They also do not match the values expected according to the supplier (see Table 1), where we see that the bending strength should be between 400 and 1000 MPa, but the samples did not exceed 400 MPa. It can be assumed that this difference in the mechanical properties of the samples is due to the presence of cracks both before and after post-impression treatment. Cracks can compromise the stability of the material when subjected to bending forces.

On the other hand, for the Al_2O_3 samples, there is a relationship with temperature. These do resemble what the supplier states in Table 1, where the range is between 200 and 500 MPa, and the samples have maximum values of 560 MPa. It should be noted that exceeding the vending strength range may be due to an experimental error.

As previously mentioned, in the case of the YSZ samples, the presence of cracks in both types of samples (see Figure 23) plays a significant role in the evaluation of flexural strength. These cracks introduce variability in the results, causing many of the measured values to deviate from the expected ones.

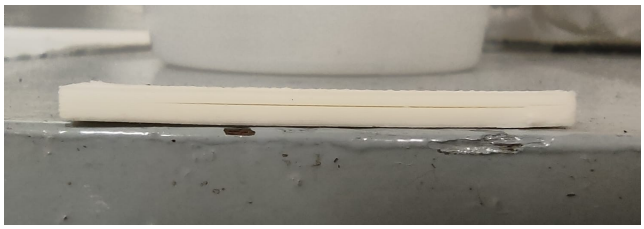

***Figure 23.** Crack observed in an Al_2O_3 sample after the sintering process.*

6. 3 RHEOLOGICAL STUDY

The rheological characterization of the YSZ and Al_2O_3 ceramic filaments was carried out to assess their suitability for extrusion-based additive manufacturing processes. To this end, viscosity and shear stress analyses were conducted as a function of shear rate (see Figure 24). The resulting curve displays a clearly pseudoplastic (shear-thinning) behavior, which is both characteristic and desirable in extrudable materials. This behavior implies that viscosity decreases as shear rate increases, facilitating extrusion during material deposition and enhancing structural stability once deposited. The viscosity at high shear rate, also known as infinite-shear

viscosity, was estimated at 11.6752 Pa·s, indicating good flowability under printing conditions. Conversely, the base viscosity, calculated at approximately 2364.11 Pa·s, reflects the initial resistance to flow under low deformation conditions.

Additionally, the material exhibits a yield stress of 1447.21 Pa, which represents the minimum stress required to initiate flow. This parameter is critical, as it helps predict the material's behavior at rest and during the onset of extrusion, playing a key role in preventing defects such as spontaneous dripping or shape loss after deposition.

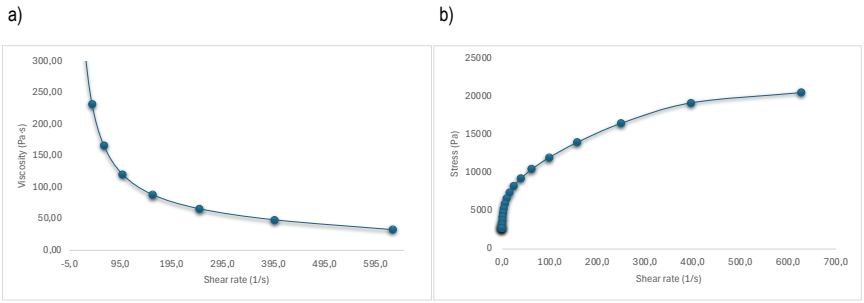

Figure 24. *Rheological behavior of the YSZ filament. Relationship between shear rate (γ) and both viscosity (η) exposed en graph (a) and between shear stress (σ) showed in graph (b).*

Overall, the results indicate that the YSZ filament exhibits optimal rheological properties for use in extrusion-based 3D printing techniques. The combination of good flowability under load and sufficient resistance at rest is essential to ensure uniform material extrusion and maintain dimensional accuracy of the samples after deposition.

6. 4 Microestructural analysis using Scanning Electron Microscopy (SEM)

A Field Emission Scanning Electron Microscopy (FE-SEM) analysis was performed on both alumina and zirconia samples. For the zirconia samples, the sintering conditions examined were: 1450 °C for 3 hours, 1500 °C for 3 hours, 1450 °C for 1 hour, and 1500 °C for 1 hour. The corresponding results are presented below.

When comparing the samples sintered at 1450 °C for 1 hour and 3 hours (see Figure 25), minimal differences are observed. Both samples appear similarly densified, with comparable grain sizes and overall microstructures. However, one notable feature that deserves closer examination is the presence of dark, well-defined shapes within the microstructure (see Figure 25(c)). In general, the images reveal the layered structure characteristic of Fused Filament Fabrication (FFF) 3D printing, along with the presence of cracks features that have notably affected the flexural strength results (see Figure 25(a) and (b)).

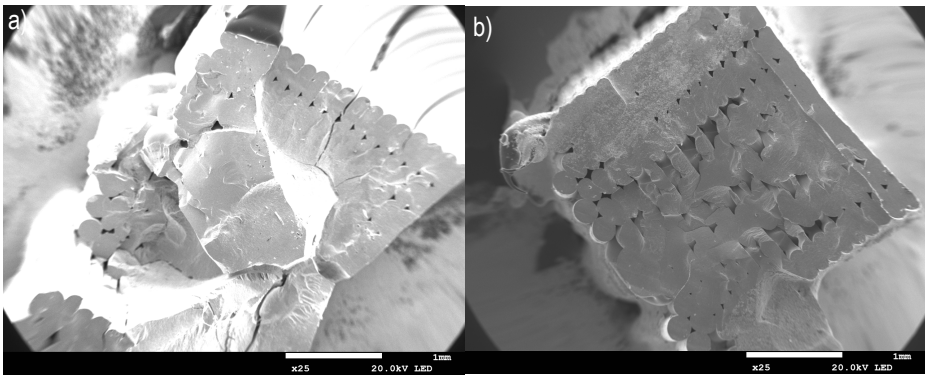

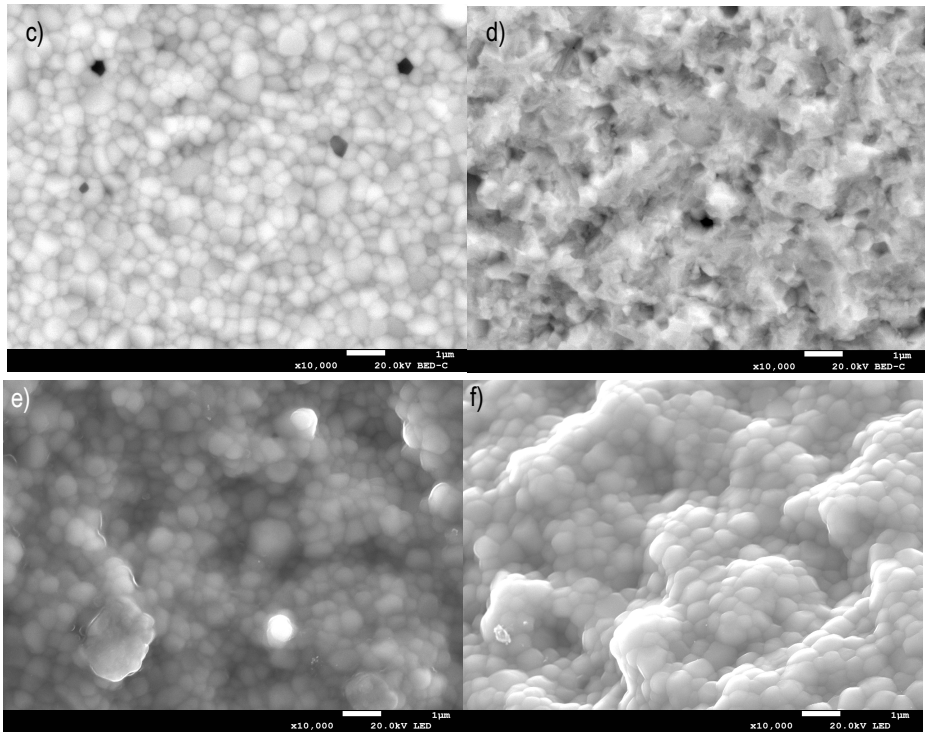

***Figure 25**. Comparative imageof YSZ 1450 1H (a,c,e) y 1450 3H (b,d,f) samples.*

The images corresponding to the YSZ samples sintered at 1500 °C for 1 hour and 3 hours are shown in Figure 26. Both samples exhibit a very similar microstructure to each other, and closely resemble those sintered at 1450 °C. In Figure 26(f), it can be observed that the grains in the 3-hour treatment reach sizes exceeding 1 µm, which are larger than those observed at 1450 °C.

Additionally, in Figures 26(e) and 26(f), the appearance of dark, square-like, well-defined regions is once again noticeable. These features contrast with the surrounding homogeneous matrix and warrant further investigation, as they may be linked to local compositional or structural variations.

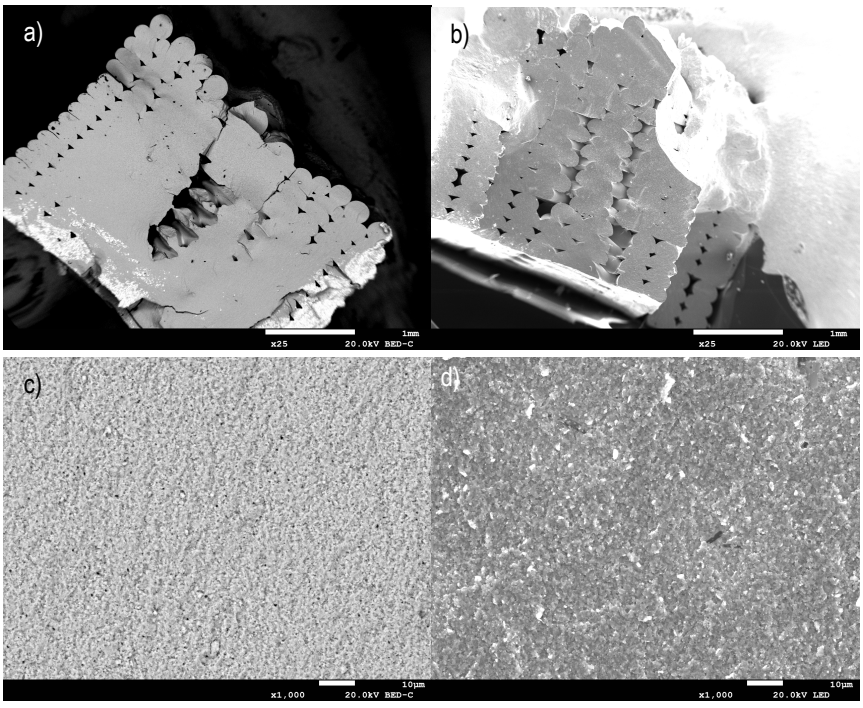

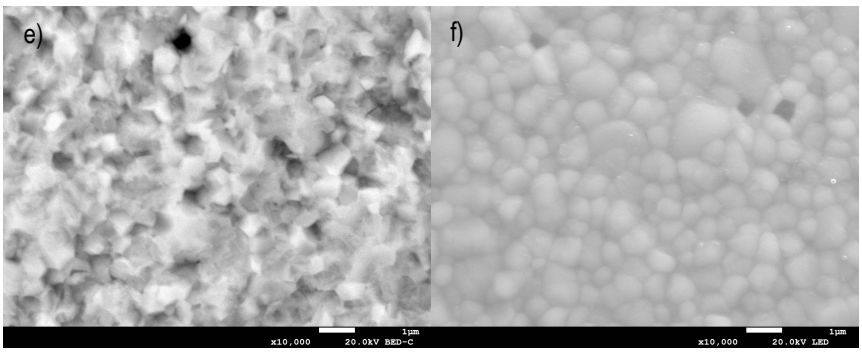

***Figure 26**. Comparative images of YSZ samples sintered at 1500 °C for 1 hour (a, c, e) and 3 hours (b, d, f).*

Due to the presence of these unusual regions that differ from the majority of the surface, a thorough analysis was conducted using SEM and Backscattered Electron Imaging (BSE). While SEM images may show darker areas that correspond to regions of similar composition, BSE images where brightness varies with the atomic number of the elements revealed the existence of two distinct phases. Consequently, an Energy Dispersive X-ray Spectroscopy (EDS) study was performed to confirm the presence of a secondary compound other than YSZ. As shown in the results (see Figure 27), aluminum (Al) was detected in the dark regions of the YSZ samples. This indicates the presence of a small amount of Al_2O_3 within the YSZ samples.

This finding could explain some of the anomalous values obtained during testing and may also be one of the factors contributing to the numerous cracks observed in the samples.

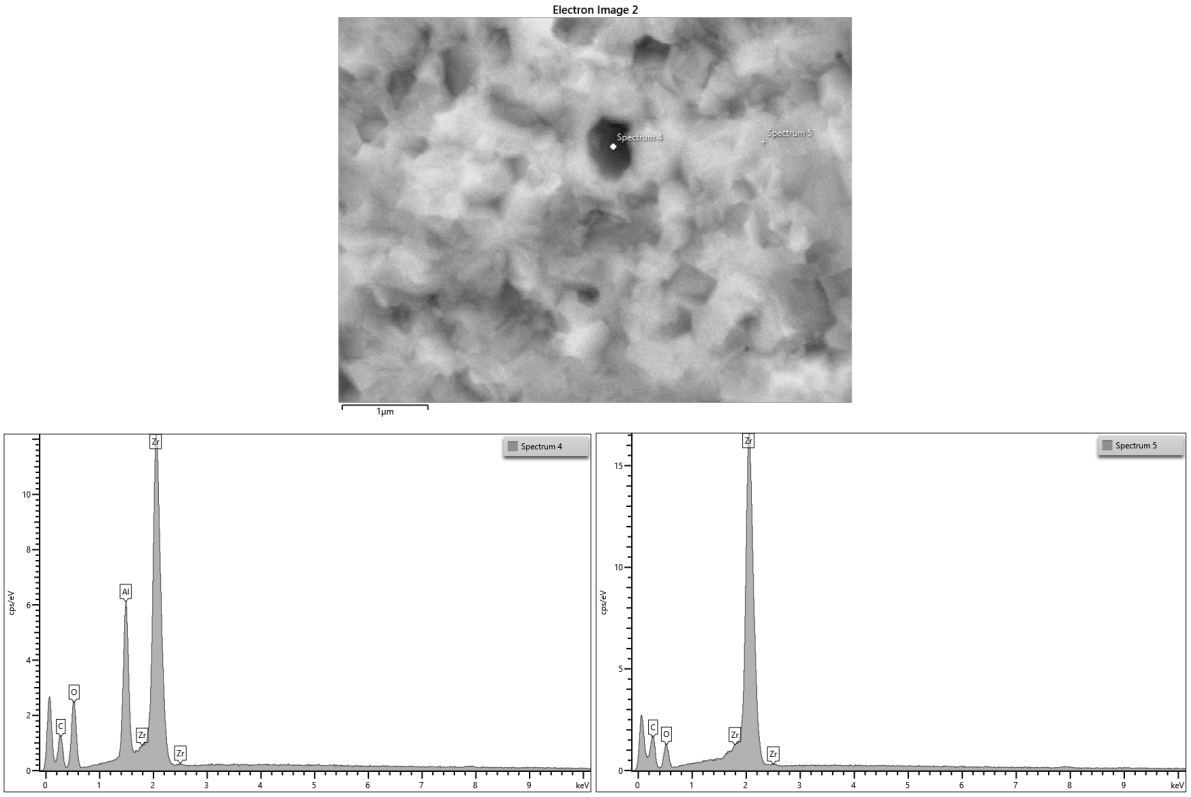

***Figure 27.** EDS analysis results: image of the studied area. Spectrum 4 corresponds to the region containing Al_2O_3, while Spectrum 5 corresponds to the homogeneous YSZ region.*

Finally, only one alumina sample was analyzed by FE-SEM (see Figure 28). Based on the images obtained, it can be concluded that grains with sizes larger than those observed in YSZ samples at both studied temperatures were formed (see Figure 29). No secondary phases other than alumina were detected, nor were any cracks observed. Relating these observations to previous analyses, it can be argued that the high flexural strength values may be associated with the larger grain size, as greater grain size typically correlates with improved mechanical resistance.

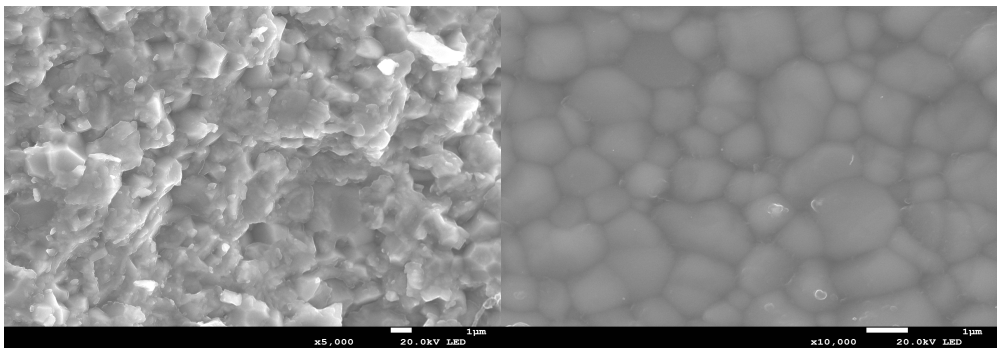

***Figure 28**. Imágenes de las muestras de Alumina 1575 3H.*

7. CONCLUSIONS

The main objective of **this research** was to determine the optimal thermal treatment conditions—including the debinding and sintering stages—for samples printed using Fused Filament Fabrication (FFF) technology, composed of YSZ and Al_2O_3, in order to achieve optimal mechanical and microstructural properties.

Thermogravimetric analyses (TGA) enabled the identification of critical degradation temperatures of the filaments, facilitating the design of suitable heating profiles for the debinding stage, during which organic binders are progressively removed without compromising the integrity of the samples. Subsequently, in the sintering phase, material consolidation and densification were achieved, with the greatest volumetric shrinkage and reduction in porosity observed during this stage. No significant changes in density were detected during debinding, confirming that this phase only involves the elimination of organic components.

Densification and porosity studies showed that temperature and dwell time during sintering significantly influence the final properties of the samples. In YSZ, sintering at 1500 °C for 1 hour yielded a favorable balance between density and porosity. In Al_2O_3, although the temperature range studied was more limited, a trend toward increased porosity with higher temperatures was observed, suggesting the need for further analysis to optimize this behavior.

Flexural tests revealed that although Al_2O_3 samples exhibited good mechanical strength, results for YSZ were not entirely conclusive due to the presence of cracks detected via SEM, which affected sample integrity and hindered a direct interpretation of the material's inherent mechanical strength. Rheological analysis of the filaments confirmed a pseudoplastic behavior ideal for 3D extrusion printing, ensuring smooth extrusion and good dimensional stability after deposition.

Finally, microstructural characterization by FE-SEM showed that YSZ contained Al_2O_3 inclusions, which may be related to crack formation and variations in mechanical properties. In contrast, Al_2O_3 displayed a homogeneous, crack-free microstructure, with larger grain sizes associated with increased flexural strength.

To complement and deepen **this research**, it is recommended to incorporate advanced microstructural analyses such as X-ray diffraction (XRD) and transmission electron microscopy (TEM), which would provide detailed information on crystalline phases and nanoscale structure. Additionally, further mechanical testing—including hardness, compressive strength, and fracture toughness—is suggested to obtain a more complete characterization of mechanical behavior under various loading conditions. Another key aspect would be the evaluation of thermal and dimensional stability through repeated thermal cycling, simulating real service conditions. Furthermore, optimizing 3D printing parameters could help reduce defects such as the observed cracks, thereby improving the initial quality of the samples before thermal treatment.

8. REFERENCES AND NOTES

1. Kulkova, J., Kulkov, I., Rohrbeck, R., et al. (2023). *Medicine of the future: How and who is going to treat us?* Futures, 103097.
2. Narin, Francis, Pinski, Gabriel, & Gee, Helene H. (1998). *La estructura del conocimiento biomédico*. *ACIMED*, *6*(2), 129-132.
3. Merola, M., & Affatato, S. (2019). *Materials for hip prostheses: A review of wear and loading considerations*. Materials, 12(4), 495.
4. S S Das and P Chakraborti 2018 IOP Conf. Ser.: Mater. Sci. Eng. 377 012177
5. Liu, Y., Huang, X., Zhang, J., Ren, X., Zhang, Z., Wang, P., ... & Liu, C. (2021). NanoZnO-modified titanium implants for enhanced anti-bacterial activity, osteogenesis and corrosion resistance. Journal of Nanobiotechnology, 19(1), 1–15.
6. Sorrentino, R., Navarra, C. O., Di Lenarda, R., Breschi, L., Zarone, F., Cadenaro, M., & Spagnuolo, G. (2019). Effects of Finish Line Design and Fatigue Cyclic Loading on Phase Transformation of Zirconia Dental Ceramics: A Qualitative Micro-Raman Spectroscopic Analysis. Materials, 12(6), 863.
7. Kongkiatkamon, Suchada, Dinesh Rokaya, Santiphab Kengtanyakich, y Chaimongkon Peampring. 2023. "Current Classification of Zirconia in Dentistry: An Updated Review." PeerJ 11: e15669.
8. Miranda, M., Marques, T., Araújo, F., Correia, A., Miranda, C., & Fernandes, M. H. (2016). *Low Temperature Degradation – Ageing of a Zirconia Dental Implant*. Presentado en IRF2016 – International Conference on Integrity – Reliability – Failure.
9. Kern, F., Lindner, V., & Gadow, R. (2016). Low-temperature degradation behaviour and mechanical properties of a 3Y-TZP manufactured from detonation-synthesized powder. Ceramics International, 42(16), 18836–18842.
10. Jiang, D., Zhao, W., Liu, Y., & Zhang, F. (2020). Low-temperature degradation of high-strength Y-TZP (yttria-stabilized tetragonal zirconia polycrystal). Dental Materials Journal, 39(4), 636–643
11. Piconi, C., & Maccauro, G. (1999). *Zirconia as a ceramic biomaterial*. Biomaterials, 20(1), 1–25.
12. Torregrosa, A., Peña, J., & Chevalier, J. (2024). Silica infiltration as a strategy to overcome zirconia degradation. Journal of Materials Science: Materials in Engineering, 15, Article 180.
13. Al-Sanabani, F. A., Madfa, A. A., & Al-Qudaimi, N. H. (2014). *Alumina ceramic for dental applications: A review article*. *1*(1).
14. Fernández, J., & Rodríguez, M. (2016). *Control de la transformación de fase γ-alúmina a α-alúmina para una densificación óptima*. *Boletín de la Sociedad Española de Cerámica y Vidrio*, 55(2), 67-74.
15. Silva, A. L., & Gómez, R. (2020). *Síntesis y caracterización de alúminas de transición a partir de desechos de aluminio reciclado. Revista Mexicana de Ingeniería Química*, 19(3), 789-796.
16. Savchenko, N. L.,Sevostyanova, I. N., Sablina, T. Y.,Molnár, L.,Géber, R., Gömze, L. A., Kulkov, S. N.,Gömze, L. N.: *The Influence of Porosity on the Elasticity and Strength of Alumina Ceramics Építőanyag*, Journal of Silicate Based and Composite Materials, Vol. 66, No. 2 (2014), 44–47. p.
17. Burger W, Kiefer G. Alumina, *Zirconia and Their Composite Ceramics with Properties Tailored for Medical Applications. Journal of Composites Science*. 2021; 5(11):306.
18. Ngo, T. D., et al. (2018). Additive manufacturing (3D printing): A review of materials, methods, applications and challenges. Composites Part B.
19. Penenrey, J., Corona, J., Rodriguez-Delgado, D., & Poblano-Salas, C. (2021*). Desde la planeación hasta la fabricación de prótesis de cadera personalizadas por manufactura aditiva de metales. Revista Colombiana de Materiales*, (20), 57–69.
20. Javaid, M., & Haleem, A. (2022). *Additive manufacturing applications in medical cases: A literature-based review*. Results in Engineering, 16, 100661.
21. Ford, S., & Despeisse, M. (2016). *Additive manufacturing and sustainability.* Journal of Cleaner Production, 137, 1573–1587.
22. Li, Y., et al. (2023). *Recent advances of additive manufacturing in implant fabrication* – A review. Applied Surface Science Advances, 18, 100462.
23. Ramisetty, Y. T., Schuster, J., & Shaik, Y. P. (2024). *Investigating the impact of 3D printing parameters on hexagonal structured PLA+ samples and analyzing the incorporation of sawdust and soybean oil as post-print fillers*. Journal of Manufacturing and Materials Processing, 8(5), 193.
24. Valino, A. D., Dizon, J. R. C., Espera Jr, A. H., Chen, Q., & Advincula, R. C. (2019). Post-processing of 3D-printed polymers. Applied Sciences, 9(4), 811.
25. Calignano, F., et al. (2019). Design of Additively Manufactured Structures for Biomedical Applications. Journal of Healthcare Engineering, 2019, 9748212.
26. Singh, S., et al. (2023). 3D printed biomedical devices and their applications. Journal of the Mechanical Behavior of Biomedical Materials, 143, 105930.
27. Álvarez-Trejo, A., Cuan-Urquizo, E., Bhate, D., & Roman-Flores, A. (2023). *Mechanical metamaterials with topologies based on curved elements: An overview of design, additive manufacturing and mechanical properties*. *Materials & Design, 233*, 112190.
28. Wang, Y., & Li, H. (2023). *Ceramics 3D printing: A comprehensive overview and applications*. Materials, 7(1), 6.
29. Zhu, Y., Wang, Q., Li, M., & Zhang, L. (2020). *Effects of solvent debinding on the microstructure and properties of 3D-printed alumina ceramics*. ACS Omega, 5(47), 30612–30619.
30. Agarwal, A., & Kumar, A. (2023). *Thermal debinding for binder burnout in metal and ceramic processing.*
31. Li, J., Xu, Z., & Chen, Y. (2024). Thermal debinding for stereolithography additive manufacturing of ceramics. Materials & Design, 240, 112030.
32. Khan, M., & Ali, M. (2023). *Additive manufacturing of advanced structural ceramics for tribological applications.* Lubricants, 13(3), 112.
33. Manikandan, R., & Raja Annamalai, A. (2022). *Tungsten-Heavy Alloy Processing via Microwave Sintering, Spark Plasma Sintering, and Additive Manufacturing*: A Review. Processes, 10(11), 2352.
34. Munir, Z. A., & Ohyanagi, M. (2021). *Unconventional Materials Processing Using Spark Plasma Sintering*. Ceramics, 4(1), 3.
35. García, J. R., Pérez, M. A., & Sánchez, L. M. (2020). *Efecto de la densificación en las propiedades mecánicas de cerámicas de alúmina. Journal of Ceramic Science and Technology*, 11(2), 129–137.
36. Wang, Y., Zhang, R., Li, H., & Liu, G. (2023). *Porosity and Mechanical Performance of Al_2O_3/ZrO_2 Composites with Different Phase Ratios*. Materials, 8(12), 517.
37. Mendes, A. M., Ribeiro, C. P., & Santos, J. (2019). *Propriedades mecánicas de cerámicas porosas de alúmina obtenidas con casca de arroz como agente pirogénico. Cerámica*, 65(375), 289–295.

9. ACRONYMS

- YSZ: Yttria-Stabilized Zirconia
- Al_2O_3: Óxido de aluminio
- SM: Substractive Manufacturing
- AM: Additive Manufacturing
- TGA: Thermogravimetric Analysis
- FFF: Fused Filament Fabrication
- STL: Standard Tessellation Language
- CAD: Computer-aided design
- SEM: Scanning Electron Microscopy
- FE-SEM: Field Emission Scanning Electron Microscopy
- BSE: Backscattered Electron
- EDS:Energy Dispersive X-ray Spectroscopy